

Article type: **Full Paper**

Manuscript ID: ic-2015-026878.R1

Title: Vanadium oxyfluorides/few layer graphene composite as high performance cathode material for lithium batteries

Musa Ali Cambaz¹, B. P. Vinayan¹, Oliver Clemens^{2,3}, Anji Reddy Munnangi¹, Venkata Sai Kiran Chakravadhanula¹, Christian Kübler^{1,2} and Maximilian Fichtner^{1,2,}*

¹Helmholtz Institute Ulm for Electrochemical Energy Storage (HIU), Helmholtzstr. 11, 89081 Ulm, Germany

²Institute of Nanotechnology, Karlsruhe Institute of Technology (KIT), P.O. Box 3640, 76021 Karlsruhe, Germany

³Technische Universität Darmstadt, Joint Research Laboratory Nanomaterials, Jovanka-Bontschits-Straße 2, 64287 Darmstadt, Germany

E-mail: maximilian.fichtner@kit.edu

Keywords: metal oxyfluorides, lithium batteries, few layer graphene, high energy density, structural rearrangement

Abstract

Metal oxyfluoride compounds are gathering significant interest as cathode materials for lithium ion batteries at the moment, due to their high theoretical capacity and resulting high energy density. In this regard, a new and direct approach is presented to synthesize vanadium oxyfluorides (VO_2F), which is phase pure. The structure of VO_2F was identified by Rietveld refinement of the powder XRD pattern. It crystallizes in perovskite type structure with a disorder of oxide and fluoride ions. The as synthesized VO_2F was tested as a cathode material for lithium batteries after being surface coated with a few layer graphene. The VO_2F delivered a first discharge capacity of 254 mAh g^{-1} and a reversible capacity of 208 mAh g^{-1} at a rate of C/20 for the first 20 cycles with an average discharge voltage of 2.84 V, yielding an energy density of 591 Wh kg^{-1} . Improved rate capability, which outperforms the previous report, has been achieved showing discharge capacity of 150 mAhg^{-1} for 1 C. The structural changes during lithium insertion and extraction were monitored by ex-situ XRD analysis of the electrodes discharged and charged to various stages. Lithium insertion results in irreversible structural change of the anion lattice from $\frac{3}{4}$ cubic close packing to a hexagonal close packing to accommodate the inserted lithium ions, but keeping the overall space-group symmetry. For the first time we revealed a structural change for the ReO_3 type structure of as-prepared VO_2F to a RhF_3 structure after lithiation /delithiation, with structural changes that have not yet been observed in previous reports. Furthermore, the new synthetic approach described here would be a platform for the synthesis of new oxyfluoride compounds.

1. Introduction

In order to meet the various requirements for current and future developments of lithium ion batteries (LIBs), performance improvements are necessary and the exploitation of novel types of electrode materials with high energy density is therefore mandatory.¹⁻³ The voltage, and energy density related thereto, of LIBs is directly linked to the electronic and the crystal structure, which is reflected in the bonding properties. In this context, metal oxides have attracted the most attention due to their versatile and rich redox chemistry, which is governed by the bonding nature of the metal to ligand (oxygen) bond (M-O bond).⁴⁻⁸ An appealing alternative are metal fluorides, in which the strong ionic character of the M - F bond offers the possibility of getting high redox potentials. However, pure metal fluorides are insulating, and exhibit sluggish kinetics and low efficiency.⁹ The tailoring of the electrochemistry by partially replacing the oxygen-ions (O^{2-}) by higher electronegative fluoride-ions (F^-) are promising approaches for designing new electrode materials.¹⁰ Mixed-anion materials like oxyfluorides represent a good compromise between the aforementioned chemistries and can lead to high redox potentials, lower polarization and good cyclic stability.¹¹⁻¹³

After the introduction of a new type of disordered rock salt type intercalation compounds Li_2MO_2F ($M=V, Cr$)^{14,15} as cathode material for LIBs, oxyfluoride chemistry has attracted a lot of attention. Furthermore, perovskite type $MO_{3-x}F_x$ ($M = Ti, Ta, Mo, W, Nb$)¹⁶⁻¹⁸ transition metal oxyfluorides crystallizing in the cubic ReO_3 structure type have been known to reversibly insert lithium. Their structure can be derived from the well-known cubic ABO_3 perovskite structure leaving all the A-sites vacant. The empty A-site substructure serves as a 3-dimensional sublattice, accessible for the intercalation of guest cations¹⁹. The first report for the intercalation of lithium into NbO_2F was published by Chowdari's group¹⁷, with an

reported capacity of $\sim 180 \text{ mAh g}^{-1}$, corresponding to the insertion of ~ 1.0 Li per NbO_2F . However, lithium insertion into ReO_3 type materials is accompanied by structural rearrangements along with a change in the Li-ion bonding and therefore in the electrochemistry.²⁰ Recent a report on the synthesis of VO_2F obtained by a solid state reaction using high pressures and temperatures of 4 GPa and 800°C appeared.²¹ The reported VO_2F had 3 wt% of unknown Impurities and is showing a first discharge capacity of 250 mAh/g in the cycling range of 2.2 V-3.9 V with severe capacity fading for prolonged cycling and kinetic limitations for higher current densities. VO_2F , due to its low weight and higher redox potential, offers a higher theoretical capacity of 262 mAh g^{-1} (with respect to the intercalation of one Li per VO_2F unit) and therefore higher gravimetric energy density compared to its analogues. In addition, it is observed that the electrochemical performances of cathode materials can significantly depend upon the conductive surface coating of active materials. Among different conductive coating materials, graphene based nanostructures are very promising due to their high surface area, excellent electronic conductivity and high mechanical stability.²²⁻²⁴

Herein, we show a new way for the synthesis of phase pure vanadium dioxyfluoride (VO_2F) obtained by an one-step mechano-chemical approach using V_2O_5 and VOF_3 as the starting precursors at room temperature. VO_2F particles were further coated with conductive few layer graphene (FLG). The resulting VO_2F -FLG composite serves from the electrochemical point of view as cathode material showing a first discharge capacity of 254 mAh g^{-1} and a reversible capacity of 208 mAh g^{-1} . Furthermore, we investigate the structural rearrangement, occurring during lithiation/de-lithiation by ex-situ XRD analysis and unveil the relationship to the RhF_3 structure, which has not been observed before for VO_2F before.

2. Experimental Section

Materials Preparation: The vanadium dioxyfluoride was synthesized by high-energy milling of stoichiometric amounts of (1.1822 g; 0.0065 mol) V_2O_5 and (0.8056 g; 0.0065 mol) VOF_3 for 20h using a Fritsch P6 planetary ball mill with 80 mL silicon nitride vial and silicon nitride balls with a ball to powder ratio 15:1. All synthesis steps were carried out under inert gas atmosphere. Few layer graphene was synthesized by the thermal exfoliation of graphite oxide at 1050 °C in argon atmosphere. Where graphite oxide was prepared by Hummer's method.²⁵ The obtained VO_2F was milled with 20 wt. % few layer graphene (FLG).

Materials Characterization: Powder XRD data were collected on a STOE Stadi P diffractometer with Mo $K\alpha_1$ ($\lambda = 0.7093 \text{ \AA}$) using Debye-Scherrer geometry. The powder samples were sealed in quartz capillary (0.5mm in diameter) under an argon atmosphere. The scanning electron microscope (SEM) and energy dispersive X-ray spectroscopy (EDS) were carried out using the instrument LEO GEMINI 1550 VP equipped with Silicon Drift Detector (OXFORD Instruments).

Transmission electron microscopy (TEM) characterization of the nanocomposite was carried out using an aberration corrected FEI Titan 80-300 operated at 300 kV equipped with a Gatan imaging filter (Tridiem 863). For (S)-TEM measurements, samples were prepared by dispersing a small amount of powder directly onto holey carbon Au grids (Quantifoil GmbH). EDX-EELS Elemental mapping of the sample was performed in the scanning transmission electron microscopy mode (STEM- HAADF) with drift correction.

Electrochemical Measurement: Electrochemical tests were carried out in Swagelok-type cell versus lithium. Electrode slurries were made of 90 wt% composite and 10 wt% polyvinylidene difluoride (PVDF) binder with N-methyl-2-pyrrolidone (NMP) as solvent. The mixed slurry was coated on an aluminum foil by doctor blade technique and dried at 120°C for 12h under vacuum. Each working electrode (12 mm diameter) contained

approximately 3 mg of active material and Li foil was used as counter electrode. LP30 from BASF (ethylene carbonate/ dimethyl carbonate, 1:1 volume ratio with 1M LiPF₆) was used as electrolyte. Cyclic voltammetry (CV) experiments for the cells have been carried out from 2.1 to 4.3 V at a scan rate of 0.1 mV s⁻¹ using a Bio-Logic VMP-3 potentiostat. Temperature controlled galvanostatic charge-discharge experiments were conducted using Arbin electrochemical workstation at the room temperature in the potential range 2.1 to 4.3 V.

3. Result and Discussion

Material Characterization

The synthesis methodology followed for vanadium oxyfluoride/few layer graphene (VO₂F/FLG) nanocomposites includes two steps: i) synthesis of pure phase of VO₂F by one-step mechano-chemical approach, (ii) surface coating of VO₂F with a conductive few layer graphene. In the first step, the VO₂F was synthesized by high-energy milling of appropriate stoichiometric amounts of V₂O₅ and VOF₃ for 20h and the formation of the pure phase of VO₂F was confirmed by powder X-ray diffraction (see the further discussion below). In the second step, few layer graphene coating on VO₂F particles was carried out by milling approach and confirmed by transmission electron microscopy (see the discussion below). The final weight ratio of VO₂F to FLG was 5:1 in the composite. It was observed that, as prepared VO₂F/FLG nanocomposite is stable in air. (See the experimental section for more details)

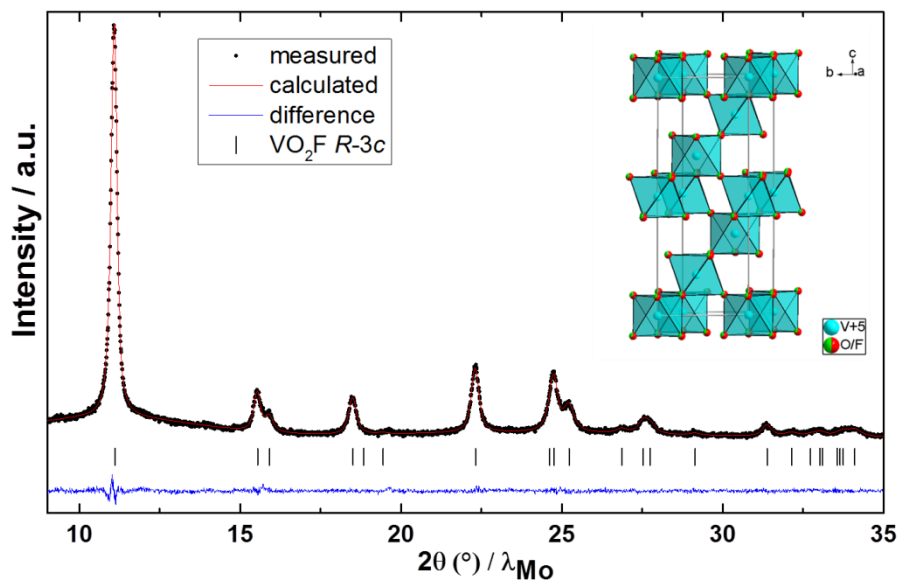


Figure 1. Rietveld refined XRD pattern of VO₂F. Inset shows the crystal structure of VO₂F.

The structure of VO₂F was determined by powder X-ray diffraction (XRD). A single phase with ReO₃ related structure was detected without the presence of impurity phases. All the reflections could be indexed using a trigonally distorted ReO₃ type phase with space group *R-3c*, which was confirmed using the Pawley method. The validity of this symmetry is clearly indicated and well supported by the appearance of the $(1\ 1\ 3)_{R-3c}$ superstructure reflection as well as the splitting pattern of the main reflections in comparison to the cubic aristotype structure with space group *Pm-3m*. This symmetry was also found for the high pressure modification of NbO₂F.²⁶ Full structural analysis was then performed using a modified structural model of NbO₂F²⁶ as starting model, refining the structural parameters. This resulted in an excellent fit of the pattern (see **Figure 1**). The refined structural data and a drawing of the crystal structure is shown in Figure 1.

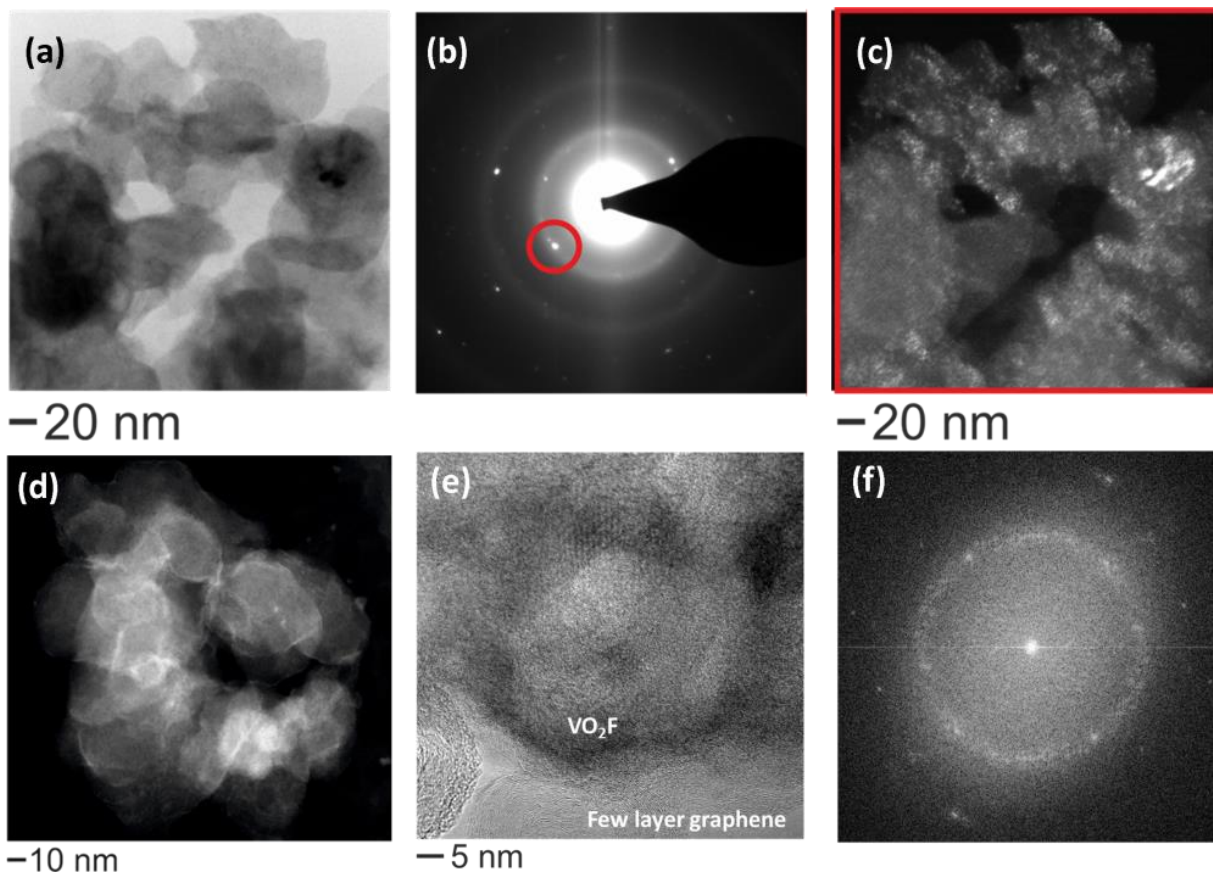


Figure 2. (a) Bright-field TEM (BF-TEM) images of VO₂F/FLG sample. (b) Selected area diffraction (SAED) pattern of the BF-TEM. (c) Dark-field TEM (DF-TEM) by using the 10 μ m aperture on the SAED reflection corresponding to 3.67 Å (012). (d) STEM-HAADF image of VO₂F/FLG sample. (e, f) High-resolution TEM micrograph of VO₂F/FLG sample with the corresponding FFT.

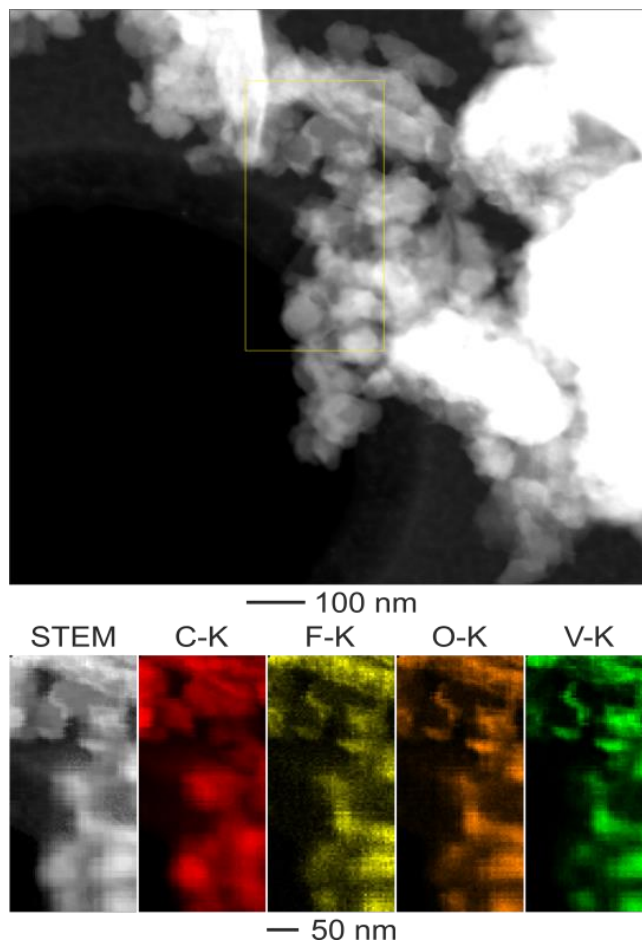


Figure 3. STEM-HAADF elemental maps of VO₂F/FLG nanocomposite.

The structural change results in nearly undistorted V(O/F)₆ octahedra (reflected by the O/F-V-O/F bond angles given in table 1) with six equal V-O/F bond distances. This bond distance agrees well with what is expected from a weighted sum of Shannon's ionic radii²⁷ ($d(\text{Shannon}) = 1.87 \text{ \AA}$ vs. $d(\text{experimental}) = 1.88 \text{ \AA}$). In contrast, the V-O/F-V bond angle of $\sim 156^\circ$ is significantly lower compared to the ideal angle of 180° for the undistorted cubic ReO₃ structure. Oxide and fluoride ions are isoelectronic and can therefore not easily be distinguished using XRD. Additionally, those ions show nearly identical scattering lengths for neutrons, making them also indistinguishable by means of powder diffraction.²⁸ No indication of ordering of those ions (e. g. by the appearance of additional superstructure reflections, further splitting of reflections or significant intensity misfit) was obtained. Disorder of oxide

and fluoride ions is a well-known phenomenon observed for many perovskite-type transition metal oxyfluorides^{29–35} which can be derived from a ccp stacking of AX₃ layers. In contrast, ordering of fluoride ions was found for many hexagonal type perovskite compounds^{36–39}. Nevertheless, the structural distortion found for VO₂F can be well understood in terms that the distortion results in a lowering of the size of the empty A-site cavities, leading to an overall decrease of cell volume and stabilization of the structural arrangement (see also discussion of lithiated compounds later in this article).

Transmission electron microscope (TEM) studies were carried out to investigate the in-depth morphology of the VO₂F/FLG (**Figure 2**). Bright-field TEM (BF-TEM) imaging (Figure 2a) of the material illustrate the composite nature of the sample. The dark contrast of VO₂F particles can be seen from the BF-TEM image and the corresponding selected area diffraction (SAED) pattern were given in Figure 2b. The *d*-values measured from the indexed SAED pattern correspond to the metrics from *R*-3*c* trigonal system VO₂F 3.67 Å (012), 2.62 Å (104), 2.56 Å (110), 2.2 Å (113), respectively from the center of the SAED pattern. Dark-field TEM (DF-TEM) by using the 10 μm aperture on the SAED reflection corresponding to 3.67 Å (012), depicts the regions of VO₂F in the DF-TEM image (Figure 2c). From the BF-TEM image, it is difficult to distinguish between carbon and VO₂F very clearly, where STEM-HAADF image (Figure 2d) shows a clear Z-contrast. Figure 2(e, f) shows the high resolution TEM micrograph along with the corresponding fast Fourier transformation (FFT). The *d*-values from the FFT (Figure 2f) correspond to aforementioned metrics from the SAED pattern (Figure 2b) and XRD data. The presence of brighter and fainter rings in the diffraction patterns (Figure 2(b, f)), indicates the polycrystalline to partly amorphous nature of the particles and corresponds to the broadened reflections observed in the XRD pattern. Furthermore, the high-resolution TEM micrograph (Figure 2e) shows that VO₂F particles were covered with few layer graphene. STEM-HAADF elemental maps of the corresponding

elements though EDX detector was shown in **Figure 3** where the V-K, O-K and F-K maps overlap with each other well. From the C-K map, it appears as if the VO₂F is embedded in a few layer graphene matrix. XPS measurements of the as synthesized sample were carried out, and confirm the V⁵⁺ oxidation state (Figure S1 supporting information). From the diffraction data, no significant deviation from an overall composition of VX₃ is noticed. This in combination with XPS measurement supports the assumption of an overall composition of VO₂F.

Electrochemical study

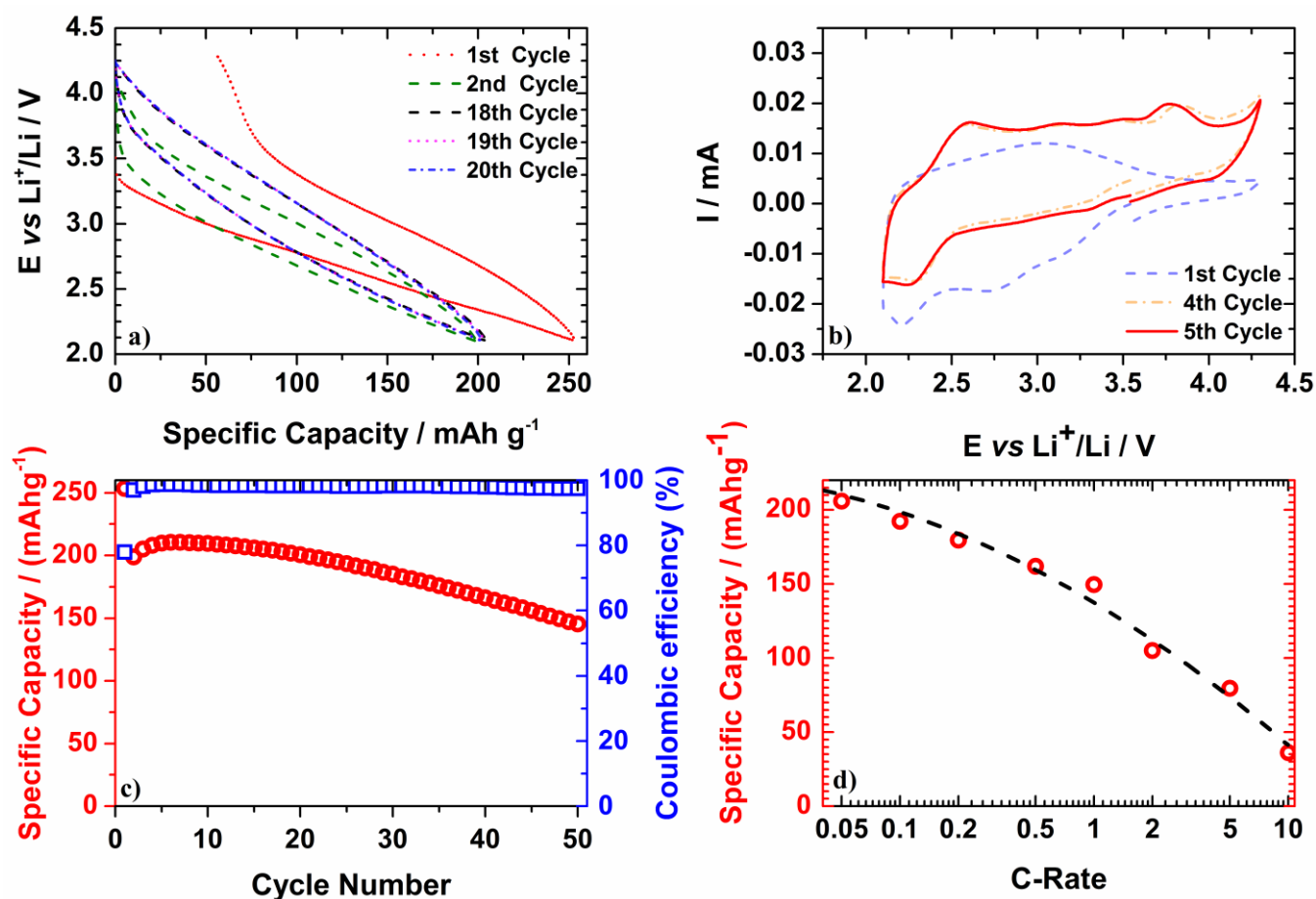


Figure 4. (a) Galvanostatic charge discharge profile of VO₂F/FLG composite in the voltage range of 2.1 and 4.3 V at a rate of C/20 rate versus Li/Li⁺(, (b) Cyclic voltammogram curve of

VO₂F/FLG composite at a scan rate with of 0.1 mVs⁻¹ (c) Cycling stability for C/20 rate between 2.1 and 4.3 V versus Li/Li⁺(d) Discharge capacities of VO₂F/FLG composite at different rates between the voltage range of 2.1 and 4.3 V versus Li/Li⁺.

Figure 4 shows typical galvanostatic discharge and charge profiles of VO₂F/FLG composite versus lithium obtained at C/20 rate (assuming the aforementioned theoretical capacity of 262 mAh g⁻¹) within the voltage range of 2.1V - 4.3V. During the first discharge, which corresponds to the insertion of lithium into the VO₂F, no plateau is visible, suggesting a solid solution system. The upcoming second cycle shows reduced polarization compared to the first one. It is interesting to note is the gradual upshift of the discharge and charge voltages, which were found to superimpose for prolonged cycling.

Figure 4 b depicts the corresponding cyclic voltammetry curves for the VO₂F/FLG composite. In the CV, for the first cathodic process broad peaks were observed at ~ 2.7 V and ~ 2.15 V, which could be attributed to the Li⁺ insertion into the crystal structure and the structural rearrangement. A broad anodic peak appears at 3.1 V, which can be assigned to the lithium deintercalation. When cycling continues the shape of the cyclic voltammetry curves change completely and CV curves tend to overlap, associated with a lower polarization. These findings suggest the occurrence of some irreversible processes in the initial cycles. The broad nature of the peaks for the initial cycles suggest indiscrete Li sites, which possibly can be attributed to disordered or amorphous phases of the VO₂F/FLG composite supported by the finding of rings in the SAED pattern (Figure 2 f) and the broadened peaks as shown in the XRD patterns. For mechano-synthesized perovskite type⁴⁰ and nanocrystalline oxide⁴¹ compounds an amorphous shell has been reported.

The cycling stability of the VO₂F/FLG composite at C/20 rate within the voltage range of 2.1-4.3 V is shown in Figure 4c. The initial discharge delivered a capacity of 254 mAh g⁻¹ suggesting an uptake of 0.97 mol Li ions per formula unit and is comparable to the obtained capacity of 250 mAh/g for C/50 rate in the literature.²¹ The subsequent charge capacity of 197 mAh g⁻¹, corresponds to the extraction of 0.75 Li ions per formula unit assuming that the capacity contribution is solely from the intercalation process. Overall 77% of the intercalated lithium ions could be deintercalated. The irreversible capacity loss was around 65 mAh g⁻¹ for the first cycle; a possible explanation will be given below. Upon further cycling the reversible capacity stabilizes at around 208 mAh g⁻¹ for the first 20 cycles, at an average discharge voltage of ~ 2.84 V compared to the recent report²¹ with around 135 mAh/g. After 10 cycles a constant decay in the capacity was observed. A similar behavior was found for the vanadium based rock salt type (space group *Fm-3m*) Li₂VO₂F¹⁴, which was synthesized in similar manner. The columbic efficiency after the 1st cycle remained around 98.4% and decreased for higher cycle numbers, which is an indication for irreversible side reactions.

After 50 cycles the test cell was disassembled and a color change was observed at the lithium side. Afterwards, the Li anode was analyzed by SEM with energy dispersive x-ray spectroscopy (EDS), the result is shown as **Figure S2** (see supplementary information). The EDS and vanadium (K_α) elemental mapping confirmed the vanadium deposition at the anode side. Vanadium dissolution and deposition at the anode side can be one of the reasons for the capacity fading during the battery operation, which was found to occur also in other vanadium based oxides.⁴² Suppression of the dissolution was partly achieved by both bulk doping⁴³⁻⁴⁵ and surface coating methods⁴⁶⁻⁴⁸

Figure 4d shows how the capacity evolved for various C rates. The specific discharge capacities at 0.02 C, 0.05 C, 0.1 C, 0.2 C, 0.5 C, 1 C, 2 C and 5 C discharge rates were 227,

206, 192, 180, 162, 150, 105, 80 mAh g⁻¹ respectively. We are showing improved capacity retention compared to the previous report²¹, which is showing a discharge capacities of around 240 mAh/g for 0.02C and around 50 mAh/g for 1 C. An increase in the current density goes along with a decrease in capacity especially for higher rates. This finding indicates kinetic limitations, which could be attributed to the low ionic or electronic conductivity. This agrees well with the observations made on electrode of VO₂F prepared without any carbon coating, which did not show any noticeable electrochemical activity. For reasons of comparability and in order to verify the impact of FLG coating, VO₂F was coated with a different carbon material (Super C65 carbon black) by a similar approach. For the latter a lower capacity retention and poorer c-rate capability (**Figure S3** see supplementary) was found.

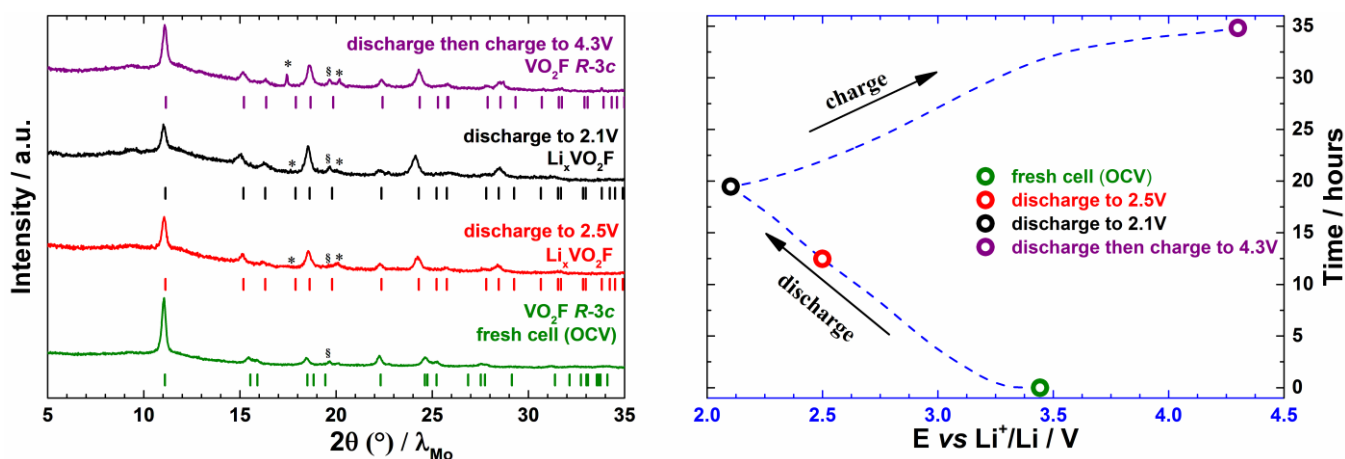


Figure 5. a) Ex-Situ XRD patterns of the electrodes collected at various discharge and charge states as shown in b). Corresponding charge-discharge profile for different lithiation / delithiation states of VO₂F/FLG composite for, which ex-situ XRD has been performed. . Peak marked with * comes from Al, which is used as current collector and § comes from the presence of a small amount of an unknown phase.

Ex-situ XRD patterns were collected on the discharged and charged electrodes in order to investigate the structural changes occurring during lithium insertion and extraction. **Figure 5a** shows the XRD patterns of the electrodes collected at different discharge and charge states as represented in Figure 5b as prepared discharged to 2.5 V, 2.1 V and recharged to 4.3 V. Structural parameters obtained from Rietveld analysis of different products were summarized in Table 1.

Table 1. Structural parameters obtained from the Rietveld analysis of as prepared cathode and the electrode discharged and charged to different voltages. Numerical standard deviations were smaller than digits given.

Compound	a [Å]	c [Å]	c/a	V [Å ³]	x(O ²⁻)	d _{avg} (V-O/F) [Å]
VO ₂ F (as-prepared)	5.12	13.09	2.56	296.7	0.42	1.88
discharged to 2.5 V	5.00	13.68	2.74	296.0	0.33	2.02
discharged to 2.1 V	4.98	13.88	2.78	298.3	0.32	2.06
charged back to 4.3 V	4.98	13.67	2.74	293.9	0.34	2.01

First of all, it is important to note that the compound reported here shows a strong change of the lattice parameters after the first discharging. The lattice parameters of the initial state were not recovered for charging the compound back. This behavior is different compared to what was found by Pérez-Flores et al.²¹. As shown in Table 2, the lattice parameters of their cell do not change to a very strong extent, and remain similar for discharged and charged state in comparison to as-prepared VO₂F of our report (compare to Table 1).

Table 2. Lattice parameters reported by Pérez-Flores et al.²¹ observed for VO₂F for different charging/discharging states

Compound	a [Å]	c [Å]	v [Å ³]	c/a
VO ₂ F (as-prepared)	5.1210(4)	13.073(2)	296.9(1)	2.55
Discharged 2.3 V	5.1162(9)	13.051(2)	295.9(1)	2.55
Charged 3.9 V	5.1190(4)	13.078(2)	296.8(1)	2.55

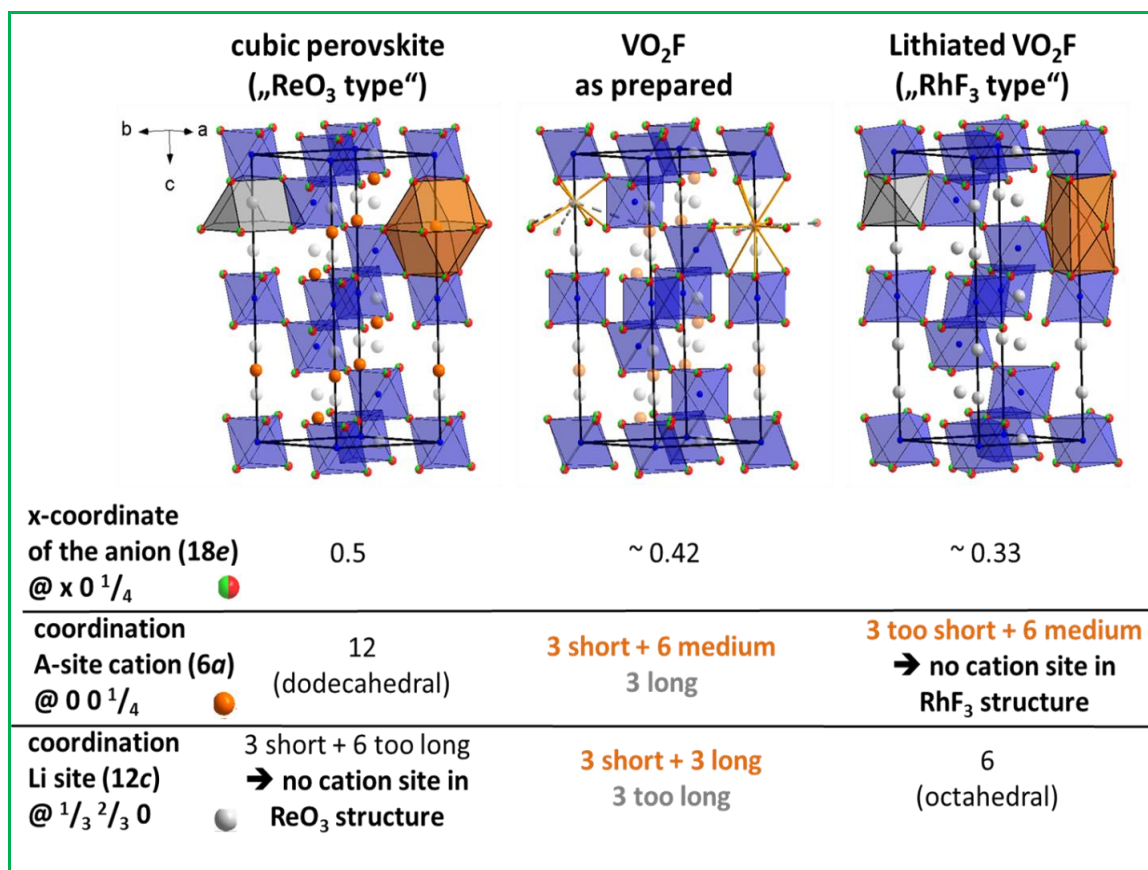


Figure 6. Crystal structure and coordination of different sites for ReO₃ type, as prepared VO₂F and lithiated VO₂F.

Therefore, it is important to derive a deeper understanding for the structural changes occurring in the VO₂F compound reported here after discharging/charging. Upon lithium incorporation into the structure, anisotropic changes of cell metrics can be observed in the XRD. The a-axis decreased and the c-axis increased on charging compared to the as prepared compound. This change was accompanied by a strong shift in the position of oxygen ions. The structural changes upon lithiation of VO₂F were therefore similar compared to the

lithiation of ReO_3 ¹⁹, which were shown in figure 6 and could be summarized as follows: the structure of VO_2F can be understood in terms of distorted cubic perovskite structure (ABX_3) with an empty A-site sub lattice. For a pseudo cubic setting of the structure, the x coordinate of the anion site must equal to $\frac{1}{2}$ and the length of the c-axis must be exactly equal to $6^{0.5} * a \sim 2.45 * a$. For pure VO_2F , the structure is already distorted to some degree ($x(\text{O}^{2-}) \sim 0.42$, $c/a \sim 2.56$). Upon lithium incorporation, we found that the c/a ratio further deviates from a value of $6^{0.5}$ (2.74 – 2.78), and that the position of the oxygen ion approaches a value of $\frac{1}{3}$. This shift of the oxygen ion results in a strong structural change, which has been described as a change from a $\frac{3}{4}$ cubic close packing (ReO_3 type structure) of anions to a hexagonal close packing of anions with $\frac{1}{3}$ occupancy of the octahedral sites (RhF_3 type structure)⁴⁹. The structural change results from the fact that basically no energetically favorable interstitial sites for Li cations would be available in the cubic ReO_3 perovskite related structure, which only possesses large 12-fold dodecahedrally coordinated sites to accommodate cations with similar sizes than the anions (e. g. alkaline earth cations). In the transition to a hcp structure ($x(\text{O}^{2-}) \rightarrow \frac{1}{3}$), additional octahedrally coordinated sites at $\frac{1}{3}$, $\frac{2}{3}$, 0 were generated, and such sites were considered to be favorable to accommodate lithium ions. Although it is difficult to locate and quantify the amount of lithium ions by means of X-ray powder diffraction data, their presence on this site is indicated when applying the Fourier difference method. Most interesting, upon de-intercalation of the lithium ions the larger c/a ratio is maintained and the x-coordinate of the oxygen ions remains close to $\frac{1}{3}$. In addition, although a significant change of cell volume is observed, parts of the lithium ions seem to remain in the structure (indicated by the larger mean V-O/F distance, i. e. reduced vanadium oxidation state). This agrees well with our observation of irreversible capacity loss in the first cycle and the change in the charge-discharge profile for the 2nd cycle. Regarding the structural analysis reported here, the VO_2F compound of this report prepared by reactive ball-milling shows a clearly different structural behavior than the compound reported by Pérez-Flores et al.²¹. This

structural change from $\frac{3}{4}$ ccp to a hcp type structure could also be the reason for differences observed in the electrochemical performance. However, the origin for the structural differences in comparison to the previous report²¹ remain unclear so far.

To check the effect of structural changes of the cathode electrode on cell impedance, EIS measurements were carried out at three different states of the cell: for the fresh cell, after first discharge to 2.1 V and after charge to 4.2 V. The Nyquist plots (**Figure S4**: supporting information) of the cell show a semicircle at high frequency region, that gives the cell resistance 'R_c' contributed by electronic/ionic resistivity of the bulk electrode and charge transfer resistance at the electrode-electrolyte interface.^{50,17} A sloping line at low frequency is connected with the diffusion of lithium ions at the cathode (Warburg region)^{50,51}. The following things were observed by comparing the diameters of the arcs of Nyquist plots, (a) an increase in the cell resistance of VO₂F cathode from fresh cell to first discharged state, and (b) after first charge, the cell resistance of VO₂F cathode was decreased considerably. The first increase of R_c could be associated with the with the formation of high intercalated film in the grain surface⁵² in VO₂F during initial lithiation. After first charging the R_c decreased as compared to the initial phase and could be due to the structural rearrangement, which is taking place as indicated by XRD. This can lead to better transport of electrons/ions within the structure as suggested by the earlier studies on the cell impedance of TiOF₂ and NbO₂F oxyfluorides.¹⁷

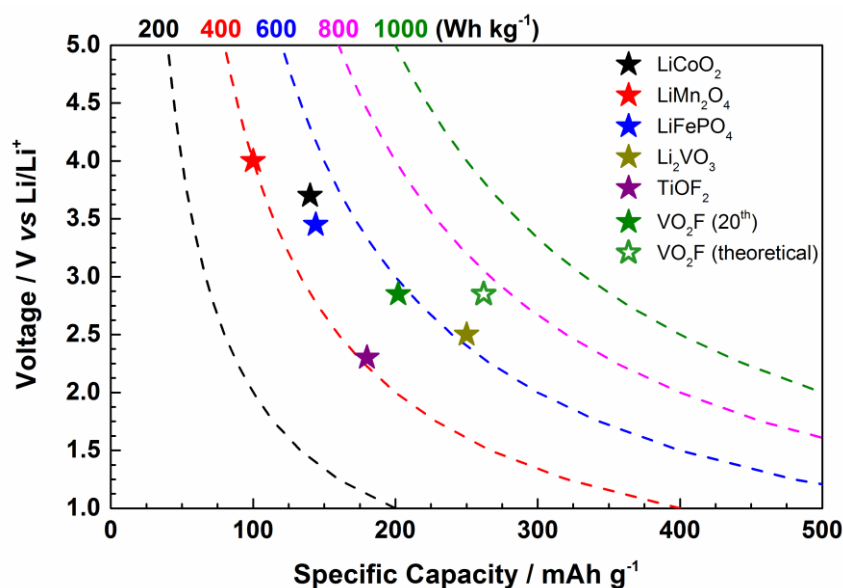


Figure 7. Specific capacity / voltage / energy density plot for various cathode materials^{16,53}

The energy density plot of new VO₂F/FLG cathode was compared with other cathode materials as shown in **Figure 7**. For the VO₂F, only the first 20 cycles have been taken into account. In relation to the well-known cathodes, the new VO₂F compound is promising and offers a possibility to achieve higher energy densities. These properties, together with the possibility to handle the material in air can make it an interesting material for further study and optimization.

3. Conclusion

In summary, we have shown a new synthesis for the synthesis of phase pure R-3c trigonally distorted VO₂F/FLG composite as cathode material and investigated the reversible lithium (de)intercalation at room temperature. A first discharge capacity of 253 mAh g⁻¹ was achieved with a reversible capacity of around 201 mAh g⁻¹ for the first 20 cycles. Compared to the previous report²¹ an improved rate capability has been achieved. The structural relationship of the VO₂F and its structural rearrangement upon lithium intercalation in relationship with the RhF₃ structure has been shown, and was evidently different compared to what has been

observed by Pérez-Flores et al.²¹ in their previous report. Upon electrochemical lithiation, the anion lattice is transforming irreversibly from a $\sqrt{3}/4$ cubic close packed to a hexagonal closed packed anion array. The structural rearrangement of VO₂F upon lithiation appears to be beneficial, lowering the polarization and due to an upshift of the output voltage. VO₂F competes well with the other cathode materials in terms of energy density. However, the cycling stability needs to be improved. Further studies are necessary to understand the change in the electrochemical profile and the capacity decay during the cycling.

Supporting Information

Refined crystal structure data, EDS, SEM and Vanadium (K_α) mapping of Li anode, EIS spectra spectra for various states, XPS, Electrochemical performance of VO₂F coated with carbon black

Acknowledgements

Financial support by EU-RTD “Hi-C” (Novel in situ and in operando techniques for characterization of interfaces in electrochemical storage systems”) in the 7th FP, grant agreement no. 608575 is gratefully acknowledged. The authors acknowledge the support by the Karlsruhe Nano Micro Facility (KNMF) for electron microscopy and spectroscopy. C.V acknowledges Dr. Christian Kübel and Prof. Dr. Horst Hahn for their continuous support.

Received: ((will be filled in by the editorial staff))

Revised: ((will be filled in by the editorial staff))

Published online: ((will be filled in by the editorial staff))

References

- (1) Tarascon, J. M.; Armand, M. *Nature* **2001**, *414* (6861), 359–367.
- (2) Armand, M.; Tarascon, J.-M. *Nature* **2008**, *451* (7179), 652–657.
- (3) Amatucci, G.; Tarascon, J.-M. *J. Electrochem. Soc.* **2003**, *150* (5), L9.
- (4) Jain, A.; Hautier, G.; Moore, C. J.; Ping Ong, S.; Fischer, C. C.; Mueller, T.; Persson, K. a.; Ceder, G. *Comput. Mater. Sci.* **2011**, *50* (8), 2295–2310.
- (5) Melot, B. C.; Scanlon, D. O.; Reynaud, M.; Rouse, G.; Chotard, J.-N.; Henry, M.; Tarascon, J.-M. *ACS Appl. Mater. Interfaces* **2014**, *6* (14), 10832–10839.
- (6) Patoux, S.; Rouse, G.; Leriche, J. B.; Masquelier, C. *Solid State Sci.* **2004**, *6* (10), 1113–1120.
- (7) Nanjundaswamy, K. *Solid State Ionics* **1996**, *92* (1-2), 1–10.
- (8) Padhi, A. K.; Archibald, W. B.; Nanjundaswamy, K. S.; Godenough, J. B. *J. Solid State Chem.* **1997**, *128* (2), 267–272.
- (9) Cabana, J.; Monconduit, L.; Larcher, D.; Palacín, M. R. *Adv. Mater.* **2010**, *22* (35), 170–192.
- (10) Rouse, G.; Tarascon, J. M. *Chem. Mater.* **2014**, *26* (1), 394–406.
- (11) Chen, R.; Ren, S.; Yavuz, M.; Guda, A. a.; Shapovalov, V.; Witter, R.; Fichtner, M.; Hahn, H. *Phys. Chem. Chem. Phys.* **2015**, *17* (26), 17288–17295.
- (12) Ko, J. K.; Wiaderek, K. M.; Pereira, N.; Kinnibrugh, T. L.; Kim, J. R.; Chupas, P. J.; Chapman, K. W.; Amatucci, G. G. *ACS Appl. Mater. Interfaces* **2014**, *6* (14), 10858–10869.
- (13) Dambournet, D.; Chapman, K. W.; Chupas, P. J.; Gerald, R. E.; Penin, N.; Labrugere, C.; Demourgues, A.; Tressaud, A.; Amine, K. *J. Am. Chem. Soc.* **2011**, *133* (34), 13240–13243.
- (14) Chen, R.; Ren, S.; Knapp, M.; Wang, D.; Witter, R.; Fichtner, M.; Hahn, H. *Adv. Energy Mater.* **2015**, *5* (9), DOI: 10.1002/aenm.201401814.
- (15) Ren, S.; Chen, R.; Maawad, E.; Dolotko, O.; Guda, A. a.; Shapovalov, V.; Wang, D.; Hahn, H.; Fichtner, M. *Adv. Sci.* **2015**, DOI: 10.1002/advs.201500128.
- (16) Louvain, N.; Karkar, Z.; El-Ghozzi, M.; Pierre, B.; Guérin, K.; Willmann, P. *J. Mater. Chem. A* **2014**, *2* (37).
- (17) Reddy, M. V.; Madhavi, S.; Subba Rao, G. V.; Chowdari, B. V. R. *J. Power Sources* **2006**, *162* (2 SPEC. ISS.), 1312–1321.
- (18) Sleight, A. W. *Inorg. Chem.* **1969**, *8* (8), 1764–1767.
- (19) Cava, R. J.; Santoro, A.; Murphy, D. W.; Zahurak, S.; Roth, R. S. *J. Solid State Chem.* **1982**, *42* (3), 251–262.
- (20) Cava, R.; Santoro, a; Murphy, D.; Zahurak, S.; Roth, R. *Solid State Ionics* **1981**, *5*, 323–326.
- (21) Pérez-Flores, J. C.; Villamor, R.; Ávila-Brandé, D.; Gallardo Amores, J. M.; Morán, E.; Kuhn, A.; García-Alvarado, F. *J. Mater. Chem. A* **2015**, *3* (41), 20508–20515.

- (22) Raccichini, R.; Varzi, A.; Passerini, S.; Scrosati, B. *Nat. Mater.* **2015**, *14* (3), 271–279.
- (23) Vinayan, B. P.; Nagar, R.; Rajalakshmi, N.; Ramaprabhu, S. *Adv. Funct. Mater.* **2012**, *22* (16), 3519–3526.
- (24) Vinayan, B. P.; Ramaprabhu, S. *J. Mater. Chem. A* **2013**, *1* (12), 3865.
- (25) William S. Hummers, J.; Offeman, R. E. *J. Am. Chem. Soc.* **1958**, *80*, 1339.
- (26) Carlson, S.; Larsson, A.-K.; Rohrer, F. E. *Acta Crystallogr. Sect. B Struct. Sci.* **2000**, *56* (2), 189–196.
- (27) Shannon, R. D. *Acta Crystallogr. Sect. A* **1976**, *32* (5), 751–767.
- (28) Clemens, O.; Slater, P. R. *Rev. Inorg. Chem.* **2013**, *33* (2-3), 105–117.
- (29) Berry, F. J.; Coomer, F. C.; Hancock, C.; Helgason, Ö.; Moore, E. A.; Slater, P. R.; Wright, A. J.; Thomas, M. F. *J. Solid State Chem.* **2011**, *184* (6), 1361–1366.
- (30) Clemens, O.; Berry, F. J.; Wright, A. J.; Knight, K. S.; Perez-Mato, J. M.; Igartua, J. M.; Slater, P. R. *J. Solid State Chem.* **2015**, *226*, 326–331.
- (31) Berry, F. J.; Heap, R.; Helgason, Ö.; Moore, E. a.; Shim, S.; Slater, P. R.; Thomas, M. F. *J. Phys. Condens. Matter* **2008**, *20* (21), 215207.
- (32) Berry, F. J.; Ren, X.; Heap, R.; Slater, P.; Thomas, M. F. *Solid State Commun.* **2005**, *134* (9), 621–624.
- (33) Clemens, O.; Berry, F. J.; Wright, A. J.; Knight, K. S.; Perez-Mato, J. M.; Igartua, J. M.; Slater, P. R. *J. Solid State Chem.* **2013**, *206*, 158–169.
- (34) Heap, R.; Slater, P. R.; Berry, F. J.; Helgason, O.; Wright, A. J. *Solid State Commun.* **2007**, *141* (8), 467–470.
- (35) Clemens, O.; Kuhn, M.; Haberkorn, R. *J. Solid State Chem.* **2011**, *184* (11), 2870–2876.
- (36) Berry, F. J.; Bowfield, A. F.; Coomer, F. C.; Jackson, S. D.; Moore, E. a; Slater, P. R.; Thomas, M. F.; Wright, A. J.; Ren, X. *J. Phys. Condens. Matter* **2009**, *21* (25), 256001.
- (37) Clemens, O.; Berry, F. J.; Bauer, J.; Wright, A. J.; Knight, K. S.; Slater, P. R. *J. Solid State Chem.* **2013**, *203*, 218–226.
- (38) Clemens, O.; Wright, A. J.; Berry, F. J.; Smith, R. I.; Slater, P. R. *J. Solid State Chem.* **2013**, *198*, 262–269.
- (39) Sturza, M.; Kabbour, H.; Daviero-Minaud, S.; Filimonov, D.; Pokholok, K.; Tiercelin, N.; Porcher, F.; Aldon, L.; Mentré, O. *J. Am. Chem. Soc.* **2011**, *133* (28), 10901–10909.
- (40) Da Silva, K. L.; Menzel, D.; Feldhoff, A.; Kübel, C.; Bruns, M.; Paesano, A.; Düvel, A.; Wilkening, M.; Ghafari, M.; Hahn, H.; Litterst, F. J.; Heitjans, P.; Becker, K. D.; Šepelák, V. *J. Phys. Chem. C* **2011**, *115* (15), 7209–7217.
- (41) Heitjans, P.; Wilkening, M. *MRS Bulletin.* 2009, 915–922.
- (42) Chernova, N. A.; Roppolo, M.; Dillon, A. C.; Whittingham, M. S. *J. Mater. Chem.* **2009**, *19* (17), 2526–2552.
- (43) Hung, F. Y.; Lui, T. S.; Liao, H. C. *Appl. Surf. Sci.* **2007**, *253* (18), 7443–7448.
- (44) Okada, M.; Lee, Y.; Yoshio, M. *J. Power Sources* **2000**, 196–200.
- (45) Shao-Horn, Y.; Middelhaugh, R. L. *Solid State Ionics* **2001**, *139* (1-2), 13–25.

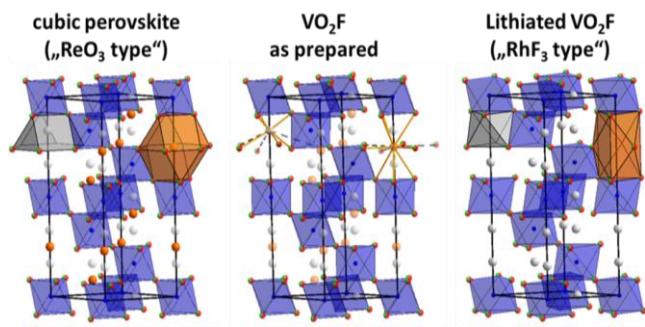
- (46) Aarik, J.; Aidla, A.; Uustare, T.; Ritala, M.; Leskelä, M. *Appl. Surf. Sci.* **2000**, *161* (3), 385–395.
- (47) Thackeray, M. M.; Johnson, C. S.; Kim, J. S.; Lauzze, K. C.; Vaughey, J. T.; Dietz, N.; Abraham, D.; Hackney, S. a.; Zeltner, W.; Anderson, M. a. *Electrochem. commun.* **2003**, *5* (9), 752–758.
- (48) Cheng, H.-M.; Wang, F.-M.; Chu, J. P.; Santhanam, R.; Rick, J.; Lo, S.-C. *J. Phys. Chem. C*, **2012**, *116*, 7629–7637.
- (49) Müller, U. *Anorganische Strukturchemie*; Teubner Studienbücher Chemie; Vieweg+Teubner Verlag: Wiesbaden, 2004.
- (50) Cui, C.; Wu, G.; Shen, J.; Zhou, B.; Zhang, Z.; Yang, H.; She, S. *Electrochim. Acta* **2010**, *55* (7), 2536–2541.
- (51) Chen, Z.; Cao, L.; Chen, L.; Zhou, H.; Xie, K.; Kuang, Y. *J. Mater. Chem. A* **2015**, *3* (16), 8750–8755.
- (52) Bohnke, C.; Fourquet, J. L.; Randrianantoandro, N.; Brousse, T.; Crosnier, O. *J. Solid State Electrochem.* **2001**, *5* (1), 1–7.
- (53) Pralong, V.; Gopal, V.; Caignaert, V.; Duffort, V.; Raveau, B. *Chem. Mater.* **2012**, *24* (1), 12–14.

For table of contents only

VO₂F few-layer graphene composite cathode was synthesized by mechanochemical approach. It's having a trigonally distorted ReO₃ type structure with the spacegroup *R-3c* and serves as an intercalation host showing a reversible capacity of 208 mA^g⁻¹ and average voltage of 2.84 V. The initial lithiation is accompanied by a structural rearrangement, which cannot be restored.

Keywords: metal oxyfluorides, lithium batteries, few layer graphene, high energy density, structural rearrangement

Title : Vanadium oxyfluorides/few layer graphene composite as high performance cathode material for lithium batteries



ToC figure